Strangeness in dense hadronic matter

Penninga, Teake Dirk

Chapter 5

Results

In Chapter 3 the calculation method of nuclear matter Lowest Order Constrained Variation was described. Then in Chapter 4 the potentials which are used in the calculation are discussed. In this chapter we will present our results for various calculations using the LOCV calculation method. First the results for the saturation curve of liquid Helium ^{3}He will be presented. Secondly the results for the Bethe homework problem will be presented. Then the results for neutron matter using realistic potentials will be given. The saturation curve of nuclear matter calculated with LOCV will be given. Finally the results for β-stable matter all or not including hyperons will be given. The resulting equations of state will then be used to construct a model of a neutron star.

5.1 Liquid helium

A well known 'difficult' manybody problem is the calculation of the equation of state of a ^{3}He liquid. Here one uses the Lennard-Jones potential [99]

$$V(r) = C\{(\frac{\sigma}{r})^{12} - (\frac{\sigma}{r})^{6}\}, \tag{5.1}$$

where $C = 40.88^{\circ}K$ and $\sigma = 2.556$ Å. Compared to the average NN and YN potentials this potential is extremely singular at the origin and is also very long ranged. It makes a very good test case for a many-body calculation method. Using just two correlation functions f^0 and f^1 the results are given in Table 5.1. The calculated values in Table 5.1 are close to the experimental value [100] of the binding energy and the saturation density.

Calculated		Experimental	
$(\frac{E}{N})_{min}(^\circ K)$	n (atoms Å^{-3})	$(\frac{E}{N})_{min}(^\circ K)$	n (atoms Å^{-3})
-1.72	0.017	-2.47 ± 0.01	0.016

Table 5.1: Saturation point ^{3}He.

The saturation curve plus the experimental binding energy at saturation density is given in Fig. 5.1.

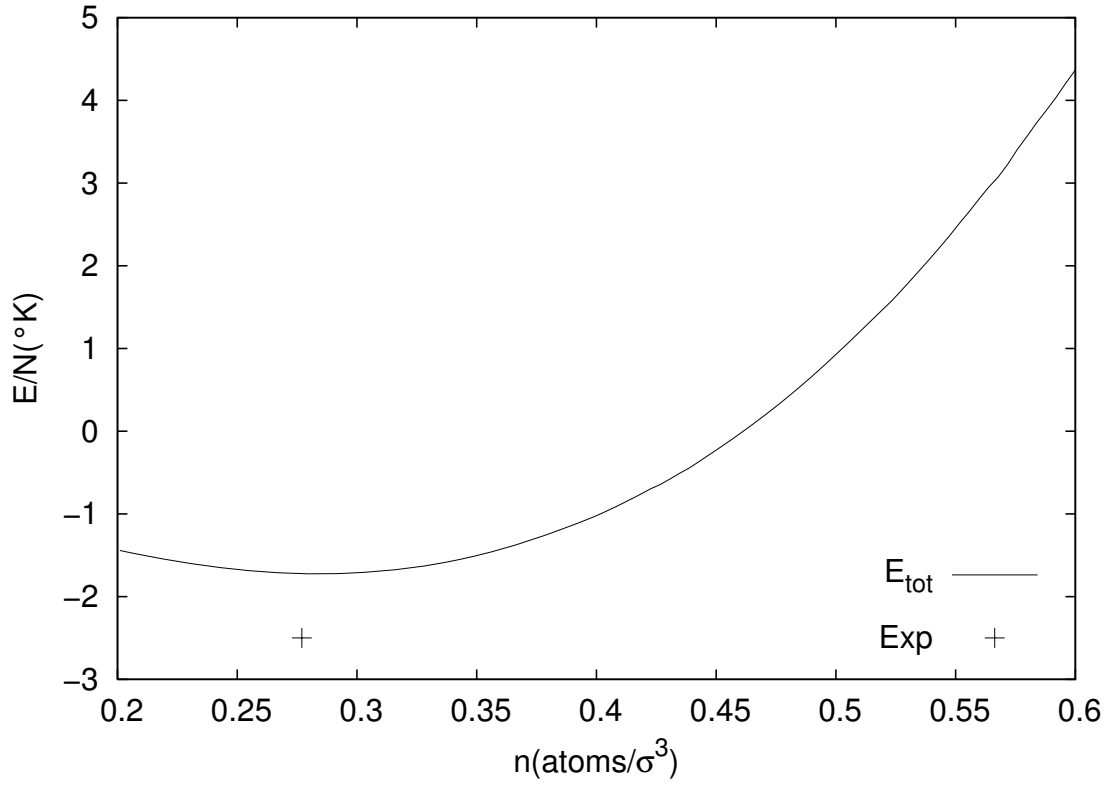

Figure 5.1: Saturation curve of ^{3}He.

The experimental error bars are well within the size of the cross.

5.2 Bethe homework model

As already noted in Chapter 1 Bethe introduced in 1973 the first of his famous homework problems. This original homework consists of a hypothetical system of neutrons interacting via the repulsive part of the Reid soft-core $^1S_0$ potential. This local potential acted in all partial waves

$$V_1(r) = 6484.2\frac{e^{-7x}}{x} \text{ MeV}, \tag{5.2}$$

where $x = 0.7r$, with r in fm. In the two following subsections results will be presented for this homework problem. First for the case where neutrons are treated as Boltzmann particles. This removes all the complications which arise from antisymmetrization when dealing with fermions. Secondly results will be presented when treating neutrons as fermions. In both cases the results will be compared to essentially correct Monte Carlo calculations taken from Refs. [101], [102] and [103].

5.2.1 Neutrons as Boltzmann particles

To further simplify the problem the neutrons are treated as Boltzmann particles. Because one is dealing with bosons the average relative momentum is zero and only the ground state ($L = 0$) has to be considered. Also the uncorrelated two-body wavefunction is a constant. So the following system has to be solved for $r < d$

$$\frac{d^2u}{dr^2} = \frac{m_n}{\hbar^2}\Big\{V_1(r) + \lambda_0\Big\}u, \tag{5.3}$$

$$f^0(r) = \frac{u(r)}{\Omega^{-\frac{1}{2}}}, \tag{5.4}$$

with the boundary condition

$$\frac{du}{dr} = 0. \tag{5.5}$$

The constraint on d is given by

$$4\pi\rho\int_0^d (f^0(r))^2 r^2 dr = 1. \tag{5.6}$$

This system is solved with a trial value for d and then with the help of Eq. (5.6) a new value of d is obtained this procedure is iterated until a self-consistent solution is obtained. The potential energy per neutron is given by

$$\frac{E_{pot}}{N} = 2\pi\rho\int_0^\infty V^0(r) r^2 dr, \tag{5.7}$$

where

$$V^0(r) = \begin{cases} -\lambda_0 (f^0(r))^2 & r < d, \\ V_1(r) & r > d. \end{cases} \tag{5.8}$$

The kinetic energy is of course zero. The resulting energy per baryon using LOCV for the homework problem is given in Fig. 5.2. As a comparison the results of the Monte Carlo calculation are also given in this figure.

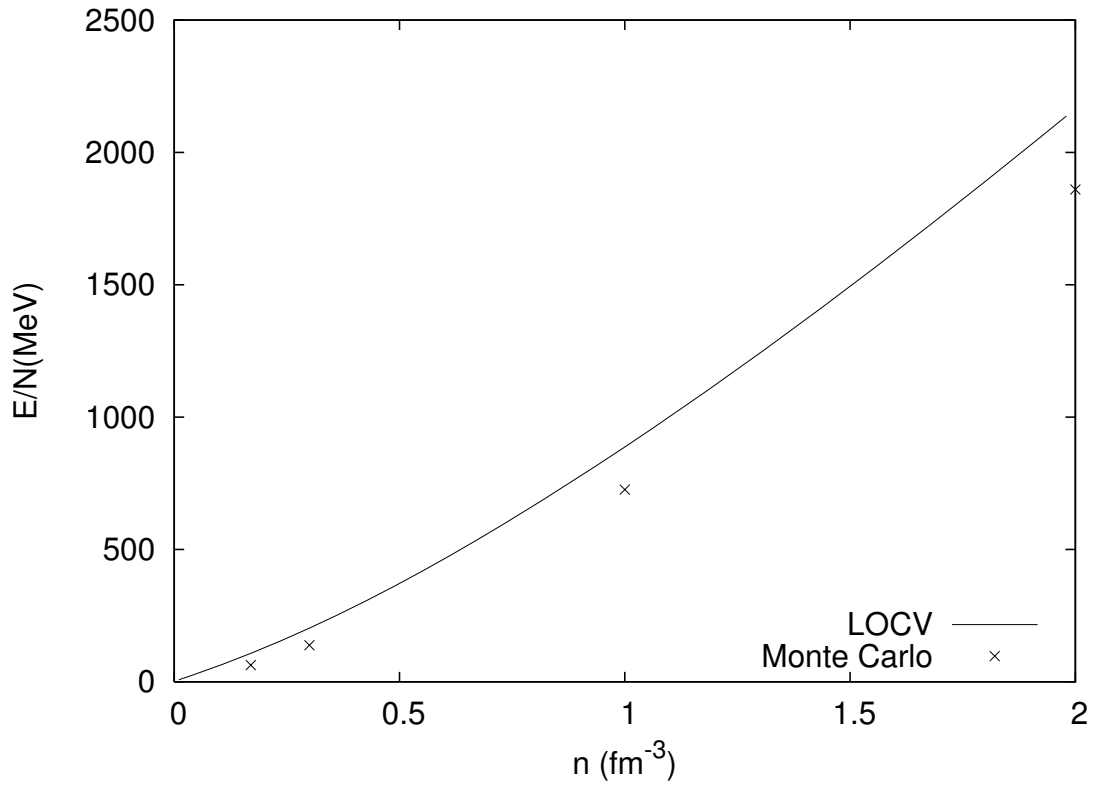

Figure 5.2: Energy as function of number density for the Bethe homework problem.

Over the whole density-range this is substantially above the results of the Monte Carlo calculations. It is possible to lower the potential energy at higher densities by increasing the healing distance d when we do not take into account constraint Eq. (5.6), but this does not help the situation at low densities. It can be argued that the homework potential is an artificial strong repulsive potential which is not encountered when calculating realistic neutron matter interactions. The range of healing distances obtained plus a typical correlation function is given in Fig. 5.3.

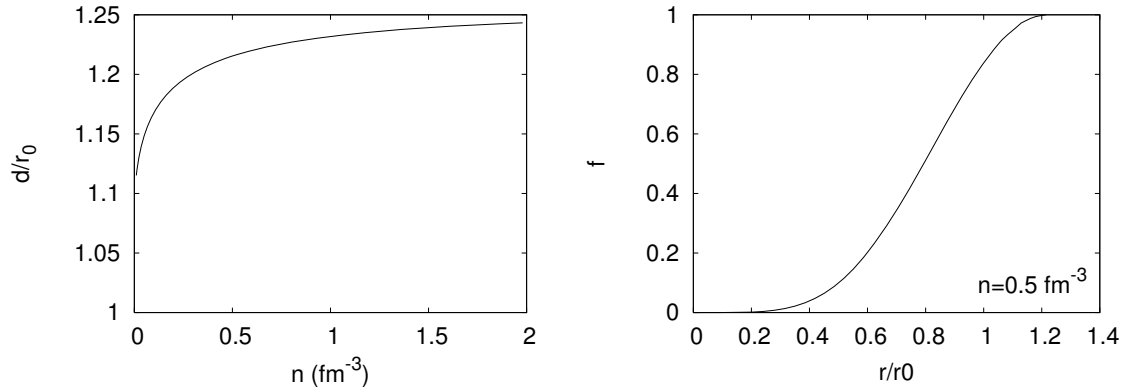

Figure 5.3: Healing distance as a function of density and a correlation function at a density of $n = 0.5\mathrm{fm}^{-3}$.

5.2.2 Neutrons as fermions

Introducing Fermi statistics but still keeping the homework potential things become a bit more complicated. One now has to use two correlation functions f^0, f^1, where f^0 is used for all even singlet partial waves and f^1 is used for all odd triplet partial waves. Because of the antisymmetrization for the even partial waves only the singlet partial waves contribute, likewise for the odd partial waves only the triplet partial waves contribute. This leads to the following system which has to be solved for $r < d$

$$\frac{d^2u_l}{dr^2} = \Big[\frac{m_n}{\hbar^2}\Big\{V_1(r) + \lambda_l\Big\} + \frac{l(l+1)}{r^2} - k_F^2,\Big]u_l, \tag{5.9}$$

$$f^l(r) = \frac{u_l(r)}{k_F r j_l(k_F r)}, \tag{5.10}$$

using the boundary condition

$$\frac{du_l}{dr} = \frac{d(k_F r j_l(k_F r))}{dr}. \tag{5.11}$$

The following constraint on d is used

$$\rho\pi \int_0^d \Big\{(f^0(r))^2 + 3(f^1)^2 - S^2(k_F r)\big[3(f^1)^2 - (f^0)^2\big]\Big\} r^2 dr = 1. \tag{5.12}$$

This system is solved with a trial value for d and then with the help of Eq. (5.12) a new value of d is obtained and this procedure is iterated until a self-consistent solution is

obtained.
The potential energy per neutron is given by

$$\frac{E_{pot}}{N} = \frac{\pi\rho}{2}\int_0^\infty \Big\{V^0(r) + 3V^1 - S^2(k_F r)\big[3V^1 - V^0\big]\Big\} r^2 dr, \tag{5.13}$$

where

$$V^l(r) = \begin{cases} -\lambda_l (f^l(r))^2 & r < d, \\ V_1(r) & r > d, \end{cases} \tag{5.14}$$

and

$$S(k_F r) = 3\frac{\sin(k_F r) - k_F r\cos(k_F r)}{(k_F r)^3}. \tag{5.15}$$

The results are given in Fig. 5.4

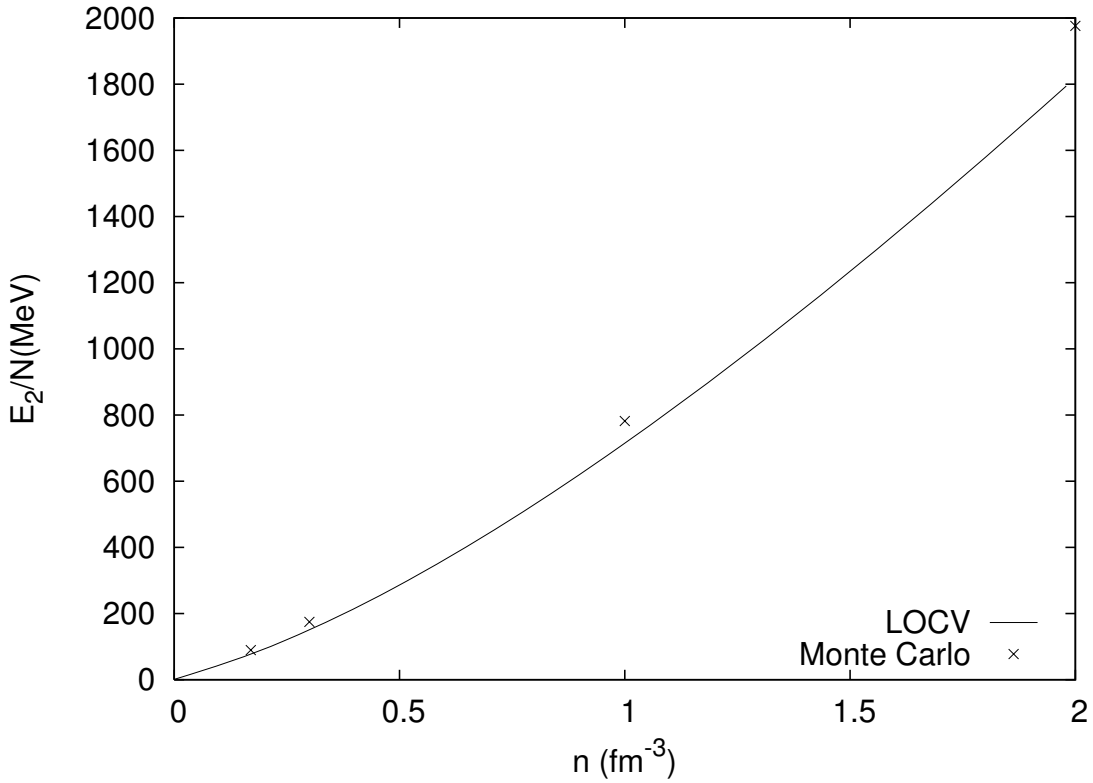

Figure 5.4: Energy per neutron as a function of number density.

Over the whole density-range this is below the results of the Monte Carlo calculations. The range of healing distances obtained plus typical correlation functions are given in Fig. 5.5.

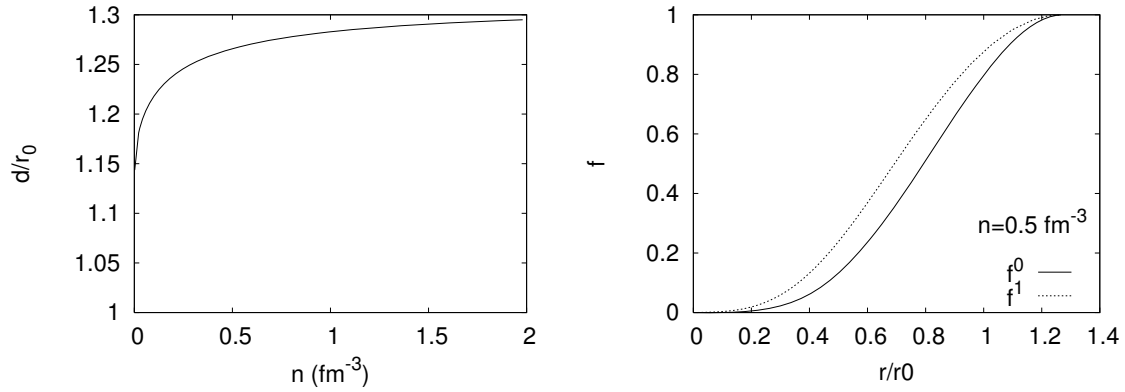

Figure 5.5: Healing distance as a function of density and odd and even correlation functions for density $n = \mathrm{fm}^{-3}$.

5.3 Neutron matter with realistic potentials

A realistic NN potential is of course much more complicated then the simple Bethe homework potential. As seen in Chapter 4 it contains spin-spin, spin-orbit and tensor operators and is in general different for each partial wave. Here the results will be presented for neutron matter for the full Reid potential, and secondly for the Nijm II potential. Let us first look at the differences between the two potentials in different partial waves which are important for neutron matter. Because of antisymmetrization requirement not all partial waves contribute. For the singlet partial waves only the $L =$ even partial waves contribute ${}^1S_0, {}^1D_2$. Likewise for the triplet partial waves only the $L =$ odd partial waves contribute ${}^3P_0, {}^3P_1, {}^3C_2 = {}^3S_2 - {}^3F_2$. The potentials for the four uncoupled partial waves is given in Fig. 5.6. The potentials in the coupled partial wave are given in Fig. 5.7 and Fig. 5.8.

The long range parts of the potential are more or less similar. But the short range behaviour of the two potentials is quite dissimilar. The Reid potential has in all partial waves a very strong repulsive core, while the NijmII potential has a much more soft repulsive core. Moreover the ${}^3P_1$ and ${}^3P_2$ partial waves for the NijmII potential have an attractive short range behaviour.

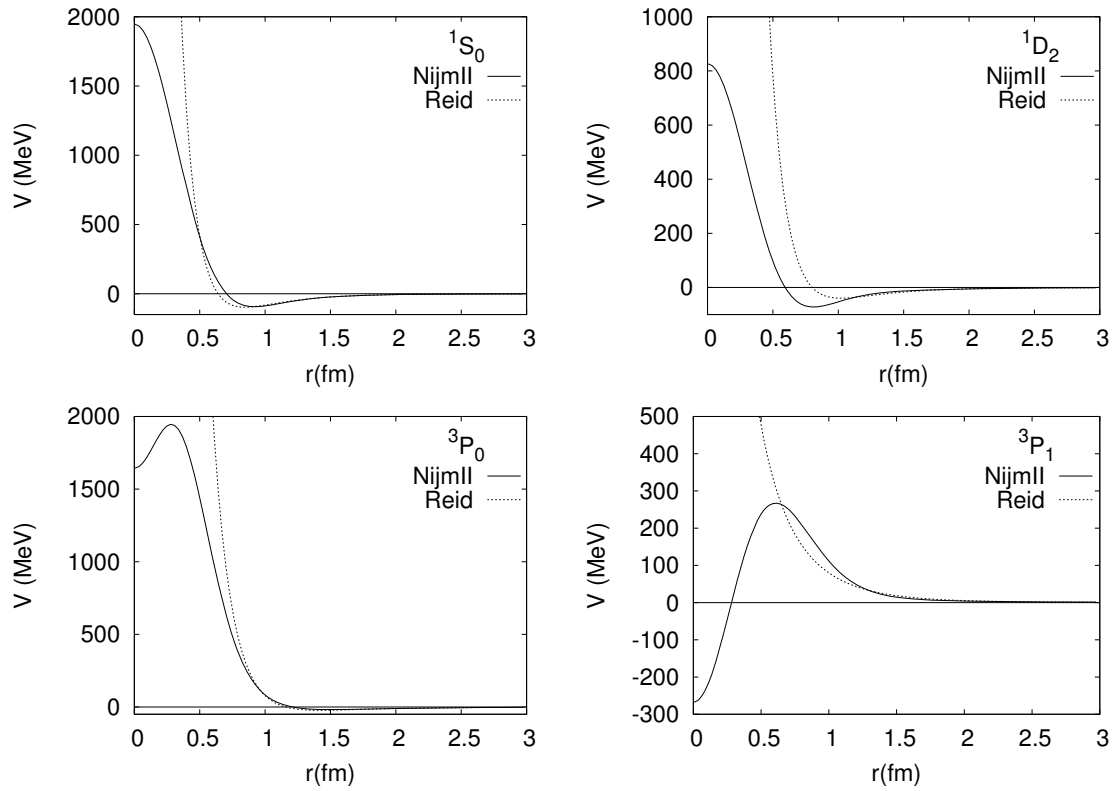

Figure 5.6: Comparison of the NN uncoupled partial waves for NijmII and Reid potential.

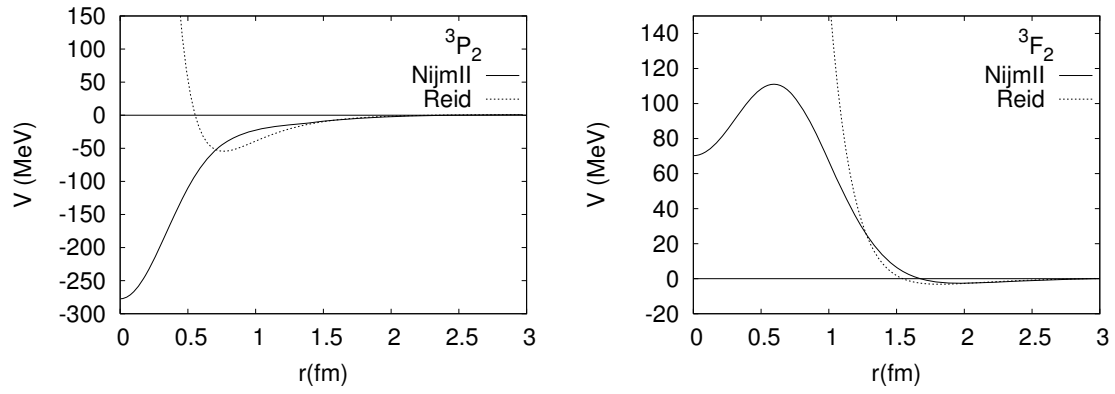

Figure 5.7: Comparison of the NN coupled partial waves for NijmII and Reid potential.

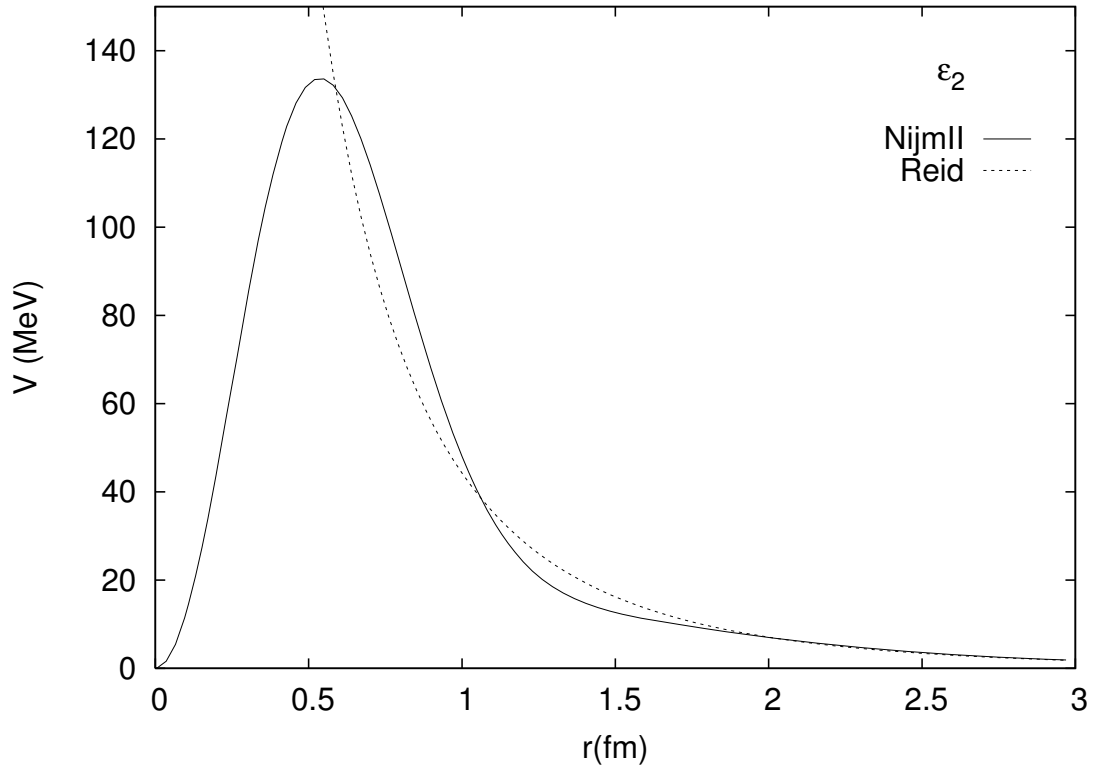

Figure 5.8: Comparison of the NN ϵ_2 partial wave for the NijmII and Reid potential.

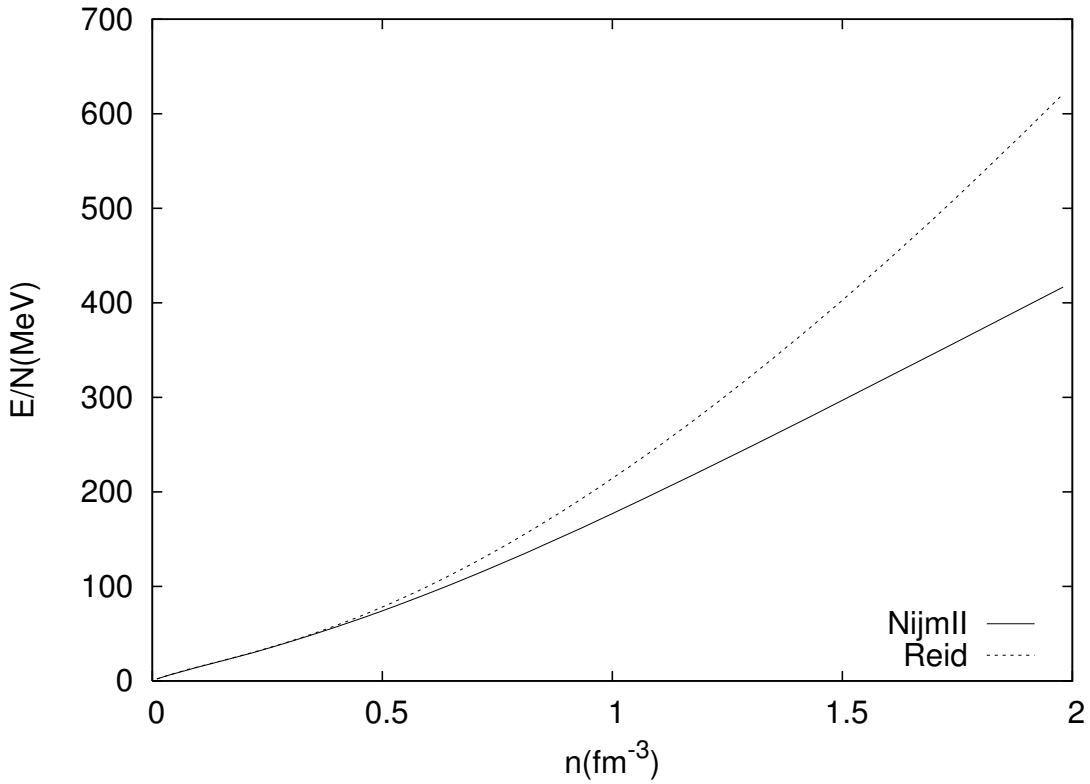

Figure 5.9: Energy of neutron matter as function of number density for the NijmII and Reid potential.

This very different short range behaviour for the two potential will significantly influence the results of the LOCV calculation. In general one would expect for low densities a more or less equal result for the calculations. But at higher densities one would expect large deviations between the two calculations. More precise one would expect that for higher density the LOCV calculation for the Reid potential would show a higher energy per neutron than the LOCV calculation for the NijmII potential. Therefore it is not surprising that the LOCV calculation for the Reid potential gives a significant higher total energy per nucleon for neutron matter especially for the higher densities as can be seen in Fig. 5.9.

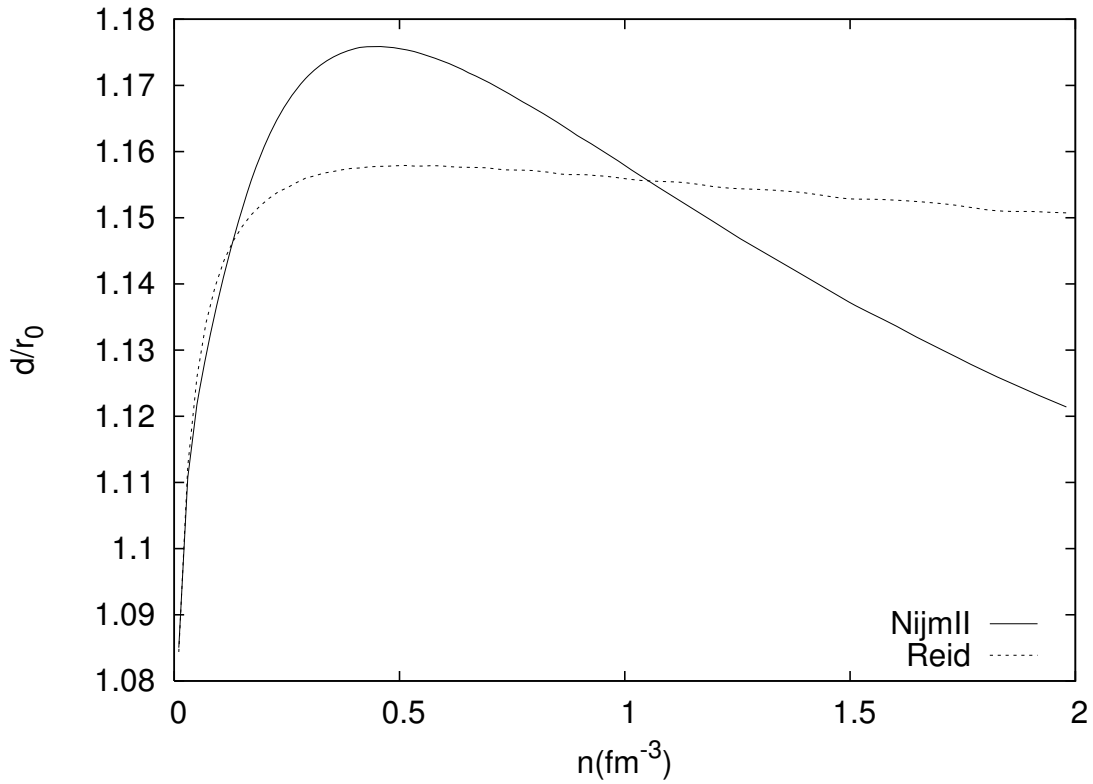

Figure 5.10: Healing distances for the NijmII and the Reid potential.

To see in more detail where these differences in total energy per nucleon come from, let us look first at the healing distances of the two potentials. The range of healing distances are given in Fig. 5.10. Here one sees that for very low density the NijmII and Reid potential have comparable healing distances. With increasing density both healing distances first increase to a maximum. The Reid potential first reaches its maximum healing distance, the NijmII potential reaches its maximum at a higher density and has a higher maximum healing distance than the Reid potential. As the density further increases this pictures changes. After their maximums both healing distances decrease with increasing density. The Reid potential healing distance decreases very slowly. Because of the very repulsive core of the Reid potential the healing distance cannot decrease very much. In contrast, the NijmII healing distance decreases more rapidly as it is not constrained by a repulsive core.

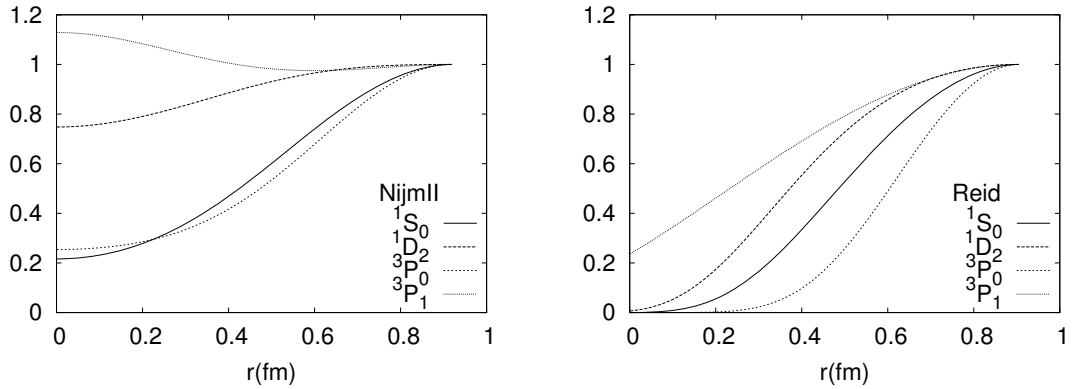

Figure 5.11: Correlation functions for uncoupled partial waves in neutron matter at a density of $n = 0.5\mathrm{fm}^{-3}$ for the NijmII and Reid potential.

Secondly one can look at the form of the various correlation functions for different partial waves. The correlation functions for $n = 0.5\mathrm{fm}^{-3}$ for the two potentials are given in Fig. 5.11 for the uncoupled partial waves and in Fig. 5.12 for the coupled partial waves. In these figures one sees distinct differences between the correlation functions for the NijmII and the Reid potential. For the Reid potential all uncoupled partial waves except for the $^3P_1$ partial wave are effectively zero in the origin, and the $^3P_1$ is small in the origin. In contrast all uncoupled partial waves for the NijmII potential are larger than zero, and the $^3P_1$ is even larger than one in the origin. For the coupled partial wave $^3C_2$ again the same picture arises for the central part of the correlation function f_C. For the Reid potential it is small in the origin. While for the NijmII potential the central part of the correlation function is in the order of one in the origin. The difference in behaviour of the correlation functions of the two potentials can again be attributed to the presence(absence) of a strong repulsive core in Reid(NijmII) potential for the different partial waves.

Finally let us look how these differences between the two potentials show up in the EoS. Up front one would expect in the low density regime, small ϵ comparable EoS's. The differences between the two EoS's should only become apparent at larger ϵ. One would expect that the EoS result from the LOCV equation for the Reid potential to be above the result of the NijmII potential. This is indeed the case as can be seen in Fig. 5.13

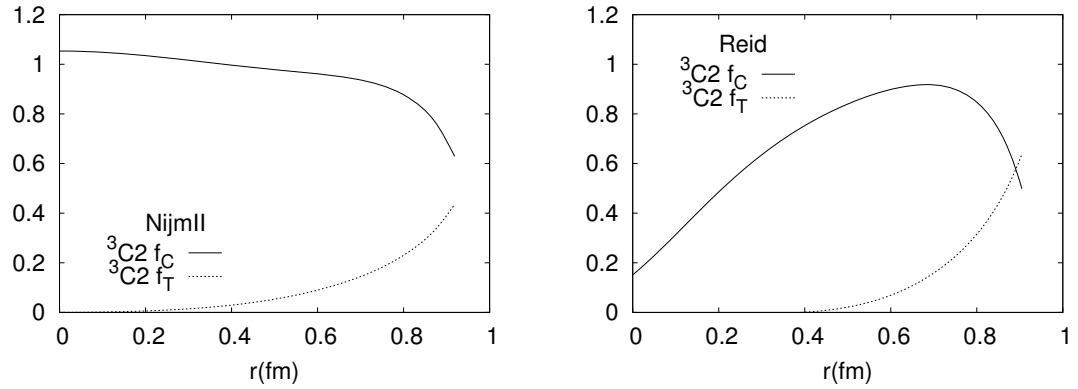

Figure 5.12: Correlation functions for coupled partial waves in neutron matter at a density of $n = 0.5\mathrm{fm}^{-3}$ for the NijmII and Reid potential.

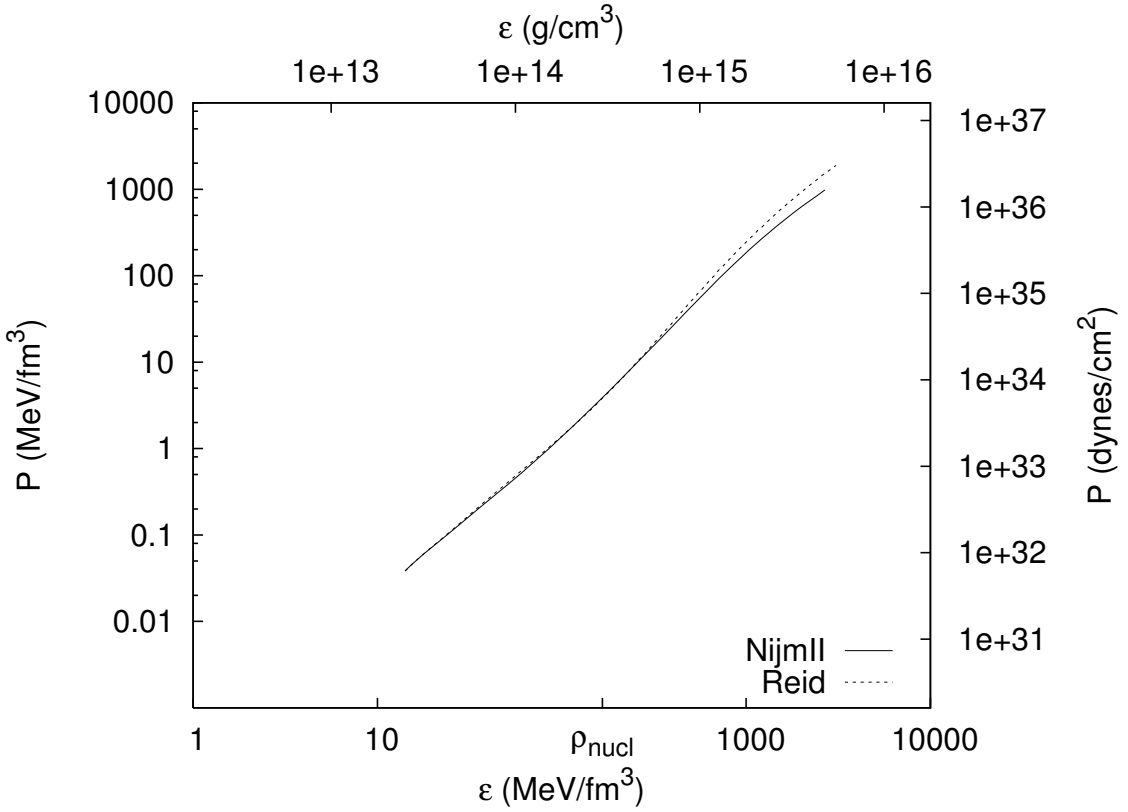

Figure 5.13: Equation of state of neutron matter for NijmII and Reid potential.

5.4 Nuclear matter with realistic potentials

Nuclear matter is a mixture of protons and neutrons. Sometimes a distinction is made between symmetric and asymmetric nuclear matter. Symmetric nuclear matter consists of equal number of protons and neutrons, whereas in asymmetric nuclear matter the number of protons and neutrons are no longer equal. In this thesis nuclear matter will always denote symmetric nuclear matter unless explicitly specified otherwise. One known fact of nuclear matter is that in contrast to neutron matter it has a saturation point. It is also known that the tensor force plays a crucial role in achieving saturation. The experimental saturation point is already given in Eq. (1.3) in Chapter 1 and is repeated in Table 5.2. So

Calculated				Experimental	
NijmII		Reid			
$\frac{E}{N}$	k_F	$\frac{E}{N}$	k_F	$\frac{E}{N}$	k_F
-6.4	1.06	-7.6	1.17	-15.7	1.36

Table 5.2: Saturation point nuclear matter ($\frac{E}{N}$ in MeV, k_F in fm^{-1}).

any manybody nuclear matter calculation should at least give saturation at a reasonable density and preferably a reasonable saturation energy. Because the saturation energy is the sum of two large terms the kinetic energy and the potential energy with different signs it is not a trivial task to obtain saturation. Here again the results for the LOCV calculation for the NijmII and Reid potential are given. In Fig. 5.14 is given the saturation curve near the calculated saturation point. From Fig. 5.14 it is clear that both LOCV calculations obtain saturation for nuclear matter. The saturation curves obtained for both potentials are not that far from the experimental saturation point. Especially when one keeps in mind that the LOCV results can only give an upper bound for the saturation energy.

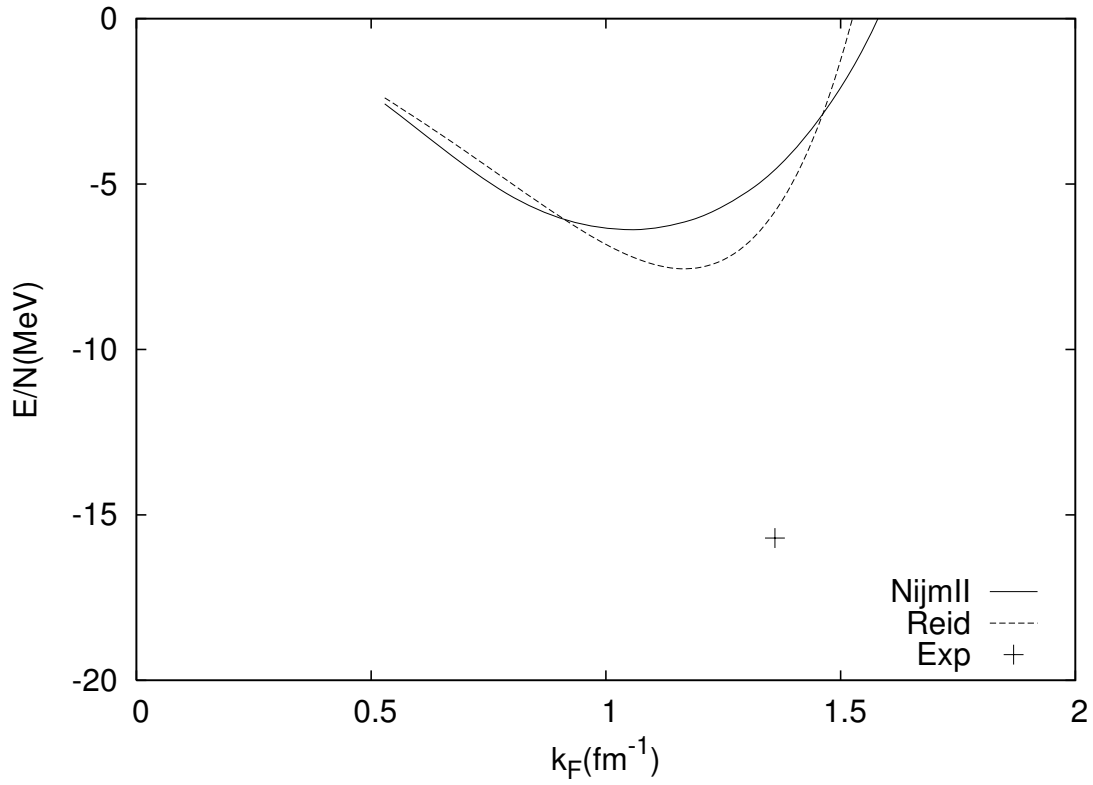

Figure 5.14: Saturation curve for nuclear matter.

To obtain a saturation curve closer to the empirical saturation curve one usually adds the so-called the Lagaris-Pandharipande 'three-body force' [104] to the RSC potential. This phenomenological potential gives for small density extra attraction which lowers the saturation point. At higher density it gives extra repulsion. This potential has the following general form

$$\begin{aligned}\tilde{V}_{\text{TNI}}(r;\rho,\beta) &= \tilde{V}_{\text{TNR}}(r;\rho) + \tilde{V}_{\text{TNA}}(r;\rho,\beta),\\ \tilde{V}_{\text{TNR}}(r;\rho) &= V_1 e^{-(r/\lambda_r)^2}(1-e^{-\eta_1\rho}),\\ \tilde{V}_{\text{TNA}}(r;\rho,\beta) &= V_2 e^{-(r/\lambda_a)^2}\rho e^{-\eta_2\rho}(\tau_1\cdot\tau_2)^2.\end{aligned} \tag{5.16}$$

Where $\lambda_r = 1.4$fm and $\eta_1 = 0.15\text{fm}^3$. The remaining parameters V_1, V_2 and η_2 are determined by the empirical saturation property and the incompressibility of symmetric nuclear matter. These parameters are given in Table 5.3 Including TNI2 in the nuclear

TNI	V_1(MeV)	V_2(MeV $\cdot$ fm^3)	η_2(fm^3)	κ(MeV)
TNI1	9.371	-22.800	14.00	200
TNI2	47.910	-17.278	11.00	250
TNI3	113.812	-14.059	8.00	300

Table 5.3: Parameters of $\tilde{V}_{\text{TNI}}$.

matter calculation leads to a lower saturation curve as can be seen in Fig. 5.15.

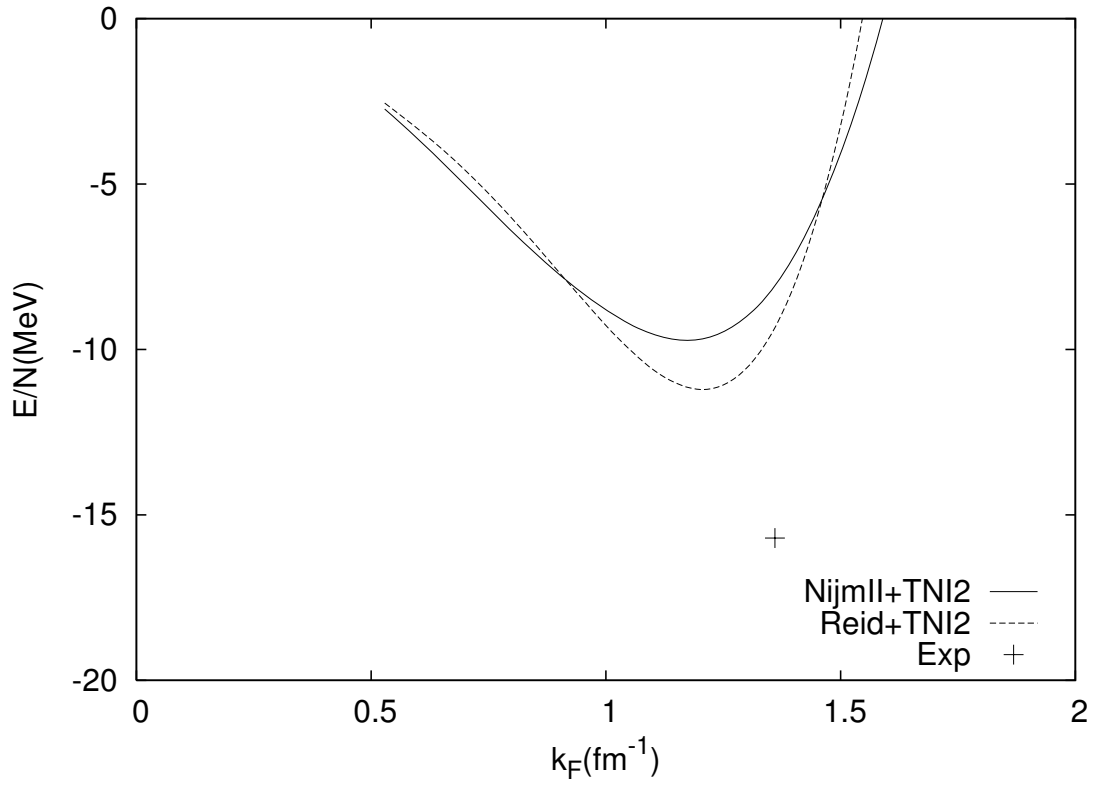

Figure 5.15: Saturation curve for nuclear matter including TNI2.

To see the crucial role the tensor force plays in achieving saturation a display of the various contributions of the partial waves to the potential energy is given. One can easily see from Fig. 5.16 that it is the $^3C_1$ partial wave which contains a strong tensor force component which shows saturation.

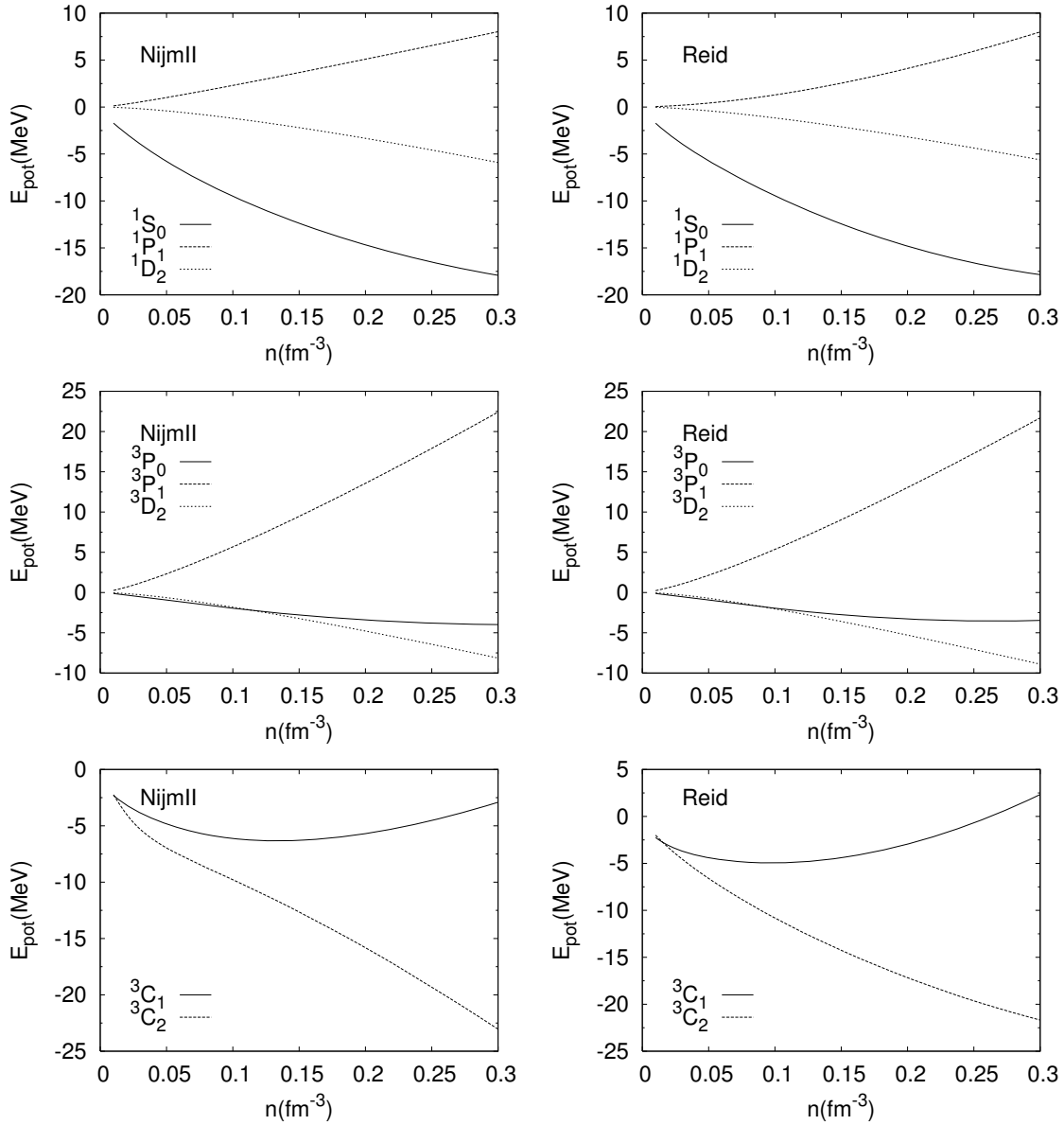

Figure 5.16: Channel breakdown of the potential energy for the NijmII and Reid potential.

In subsequent calculations the Lagaris-Pandharipande 'three-body force' is not included.

5.5 β-stable nuclear matter

In this section the concentrations of the various particles will no longer be fixed. Here we will now use chemical equilibrium to determine the concentrations of the various particles. These concentrations will vary with the density. Just as in Chapter 2 we will take a system consisting of neutrons, protons, electrons and muons. But in contrast to Chapter 2 now the strong interaction is included. Initially at low density the systems consists primarily of neutrons, but as the density increases it becomes energetically favorable to convert neutrons in protons via β-decay. The chemical potential of the electrons also increases with increasing density and at a certain density this becomes larger than the rest mass of the muon. Electrons are then converted into muons and the concentration of electrons will decrease. At high density the muon concentration will approach the electron density. The results for the Reid potential are given in Fig. 5.17.

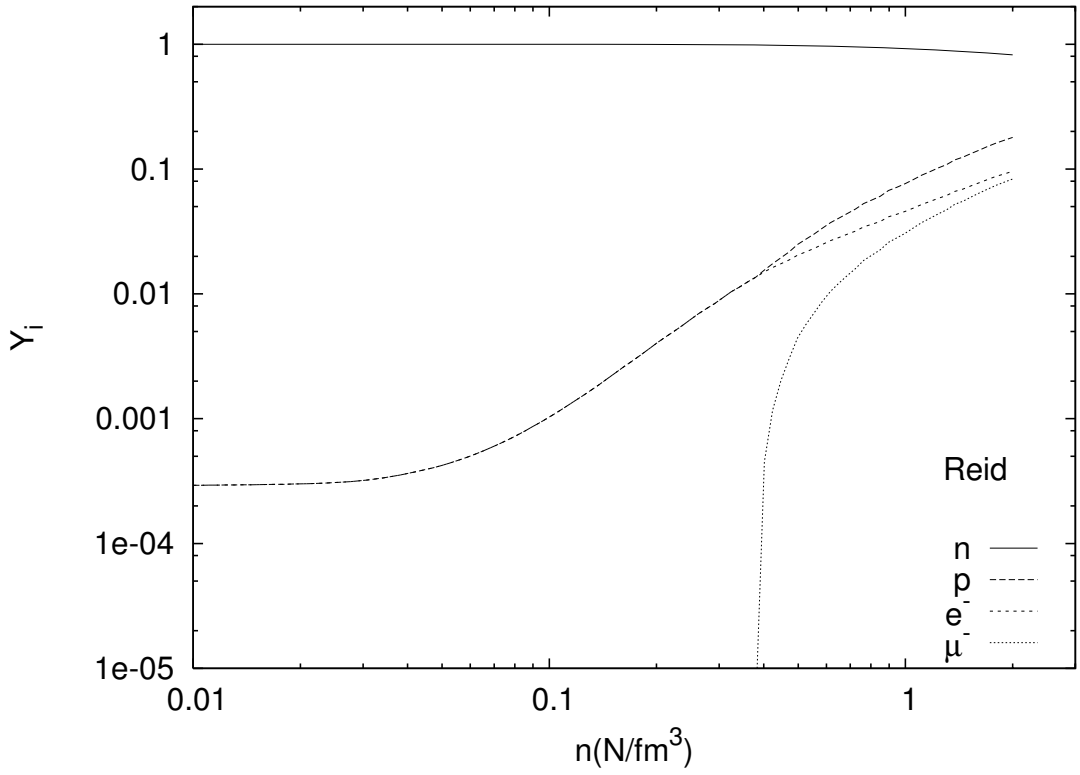

Figure 5.17: Composition of β-stable nuclear matter using the Reid potential.

The corresponding results for the NijmII potential can unfortunately not be shown. As noted earlier in this chapter the NijmII is a significantly softer short range (=high density)

potential. This keeps the chemical potential of the neutrons much lower a higher density. This results in β-stable matter only consisting of neutrons with no protons, electrons and muons present. Especially the partial waves ($^3P_1$,$^3P_2$) with an attractive potential at the origin give problems. Originally the LOCV-method was constructed with the RSC-potential in mind which is repulsive in the origin for all partial waves. This ensures that the correlation function is small in the origin. Adding the Lagaris-Pandharipande 'three-body force' to the NijmII potential adds some repulsion at the origin. But this is not enough to obtain a repulsive potential at the origin. The extra repulsion at the origin is given in Fig. 5.18.

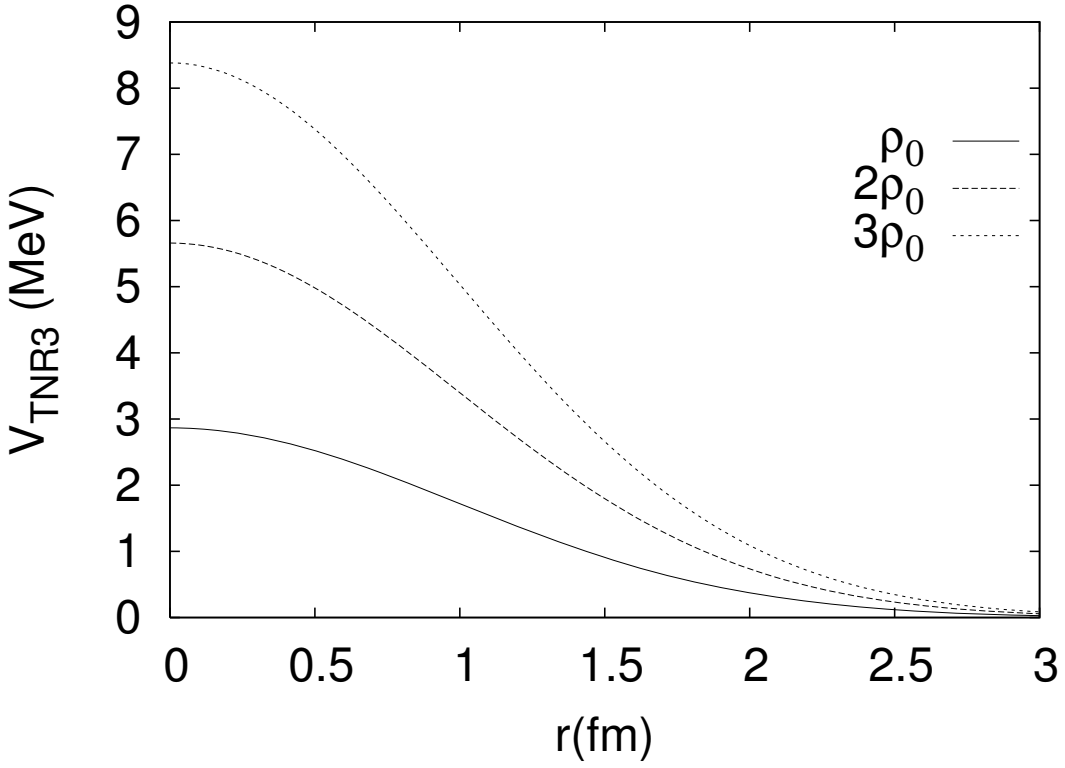

Figure 5.18: Repulsive contribution of the V_{TNI3} for various densities.

In the next few paragraphs one will compare the results for β-stable matter with or without including the Reid potential. The energy per baryon minus the rest mass of the neutron for the Reid potential is given in Fig. 5.19.

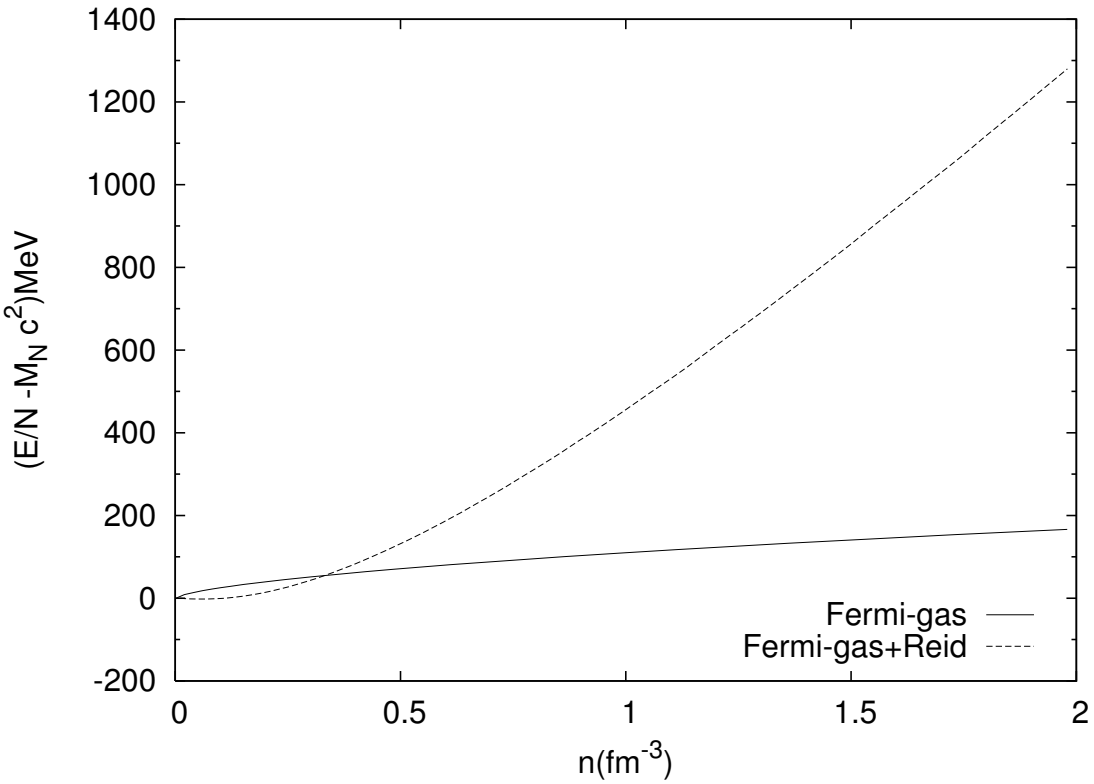

Figure 5.19: Energy for β-stable matter as function of number density with our without the Reid potential.

This nicely illustrates the influence of the Reid potential. At low density the potential is attractive resulting in a lowering of the energy. As the density increases beyond two times nuclear density the potential becomes more and more repulsive. This results in a higher energy compared to the case without the Reid potential

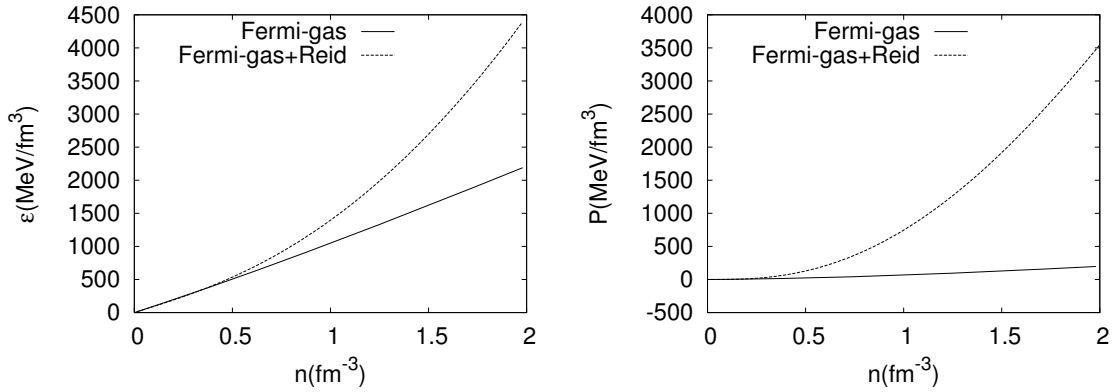

Figure 5.20: Energy density and Pressure as function of number density.

The energy density and pressure show the same features. The energy density for low density is more are less equal for the two cases, and slowly increases linearly with the number density. As soon as the number density increases above three times nuclear density the energy density of β-stable matter with the Reid potential increases much more rapidly, while the case without the Reid potential keeps increasing linearly with the number density. The pressure shows the same behaviour only here the difference between with or without the Reid potential is much more dramatically.

Finally the equation of state for β-stable nuclear matter is given in Fig. 5.21 From the previous Figures it becomes clear that for low density, the inclusion of the Reid potential softens the EoS. While at the same time the EoS becomes a lot stiffer for higher density. This situation can of course change when one incorporates hyperons.

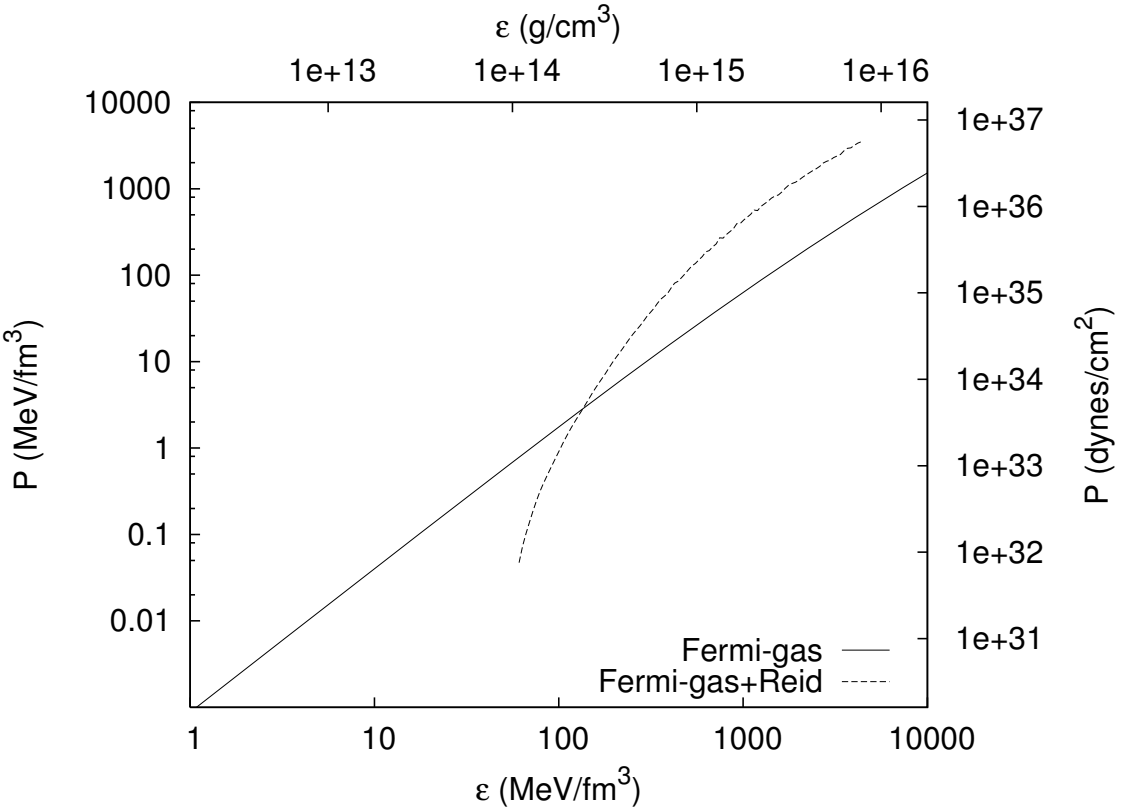

Figure 5.21: Equation of state of β-stable nuclear matter.

5.6 β-stable hyperon matter

The picture changes somewhat when one introduces also hyperons. For the nucleon-nucleon interaction again the Reid-potential is used. For the hyperon-nucleon-interaction the Reid neutron-proton potential is used. As described in 2.2.4, at low density it is energetically not allowed to have hyperons in the baryon liquid, therefor at low density one starts with a mixture of neutrons, protons and electrons. The chemical equilibrium is calculated at a certain density. Then a Λ is added with a small concentration and it is checked if the resulting chemical equilibrium has a solution. If not then the Λ is removed. The same procedure is used for the Σ^- and the μ. Then the density is increased and the whole procedure is repeated. If at a certain threshold density a fermion species can be added it is kept in the fermion liquid until the concentration of the fermion species drops below a minimum concentration it is then removed. The concentrations of the various fermions can be seen in Fig. 5.22.

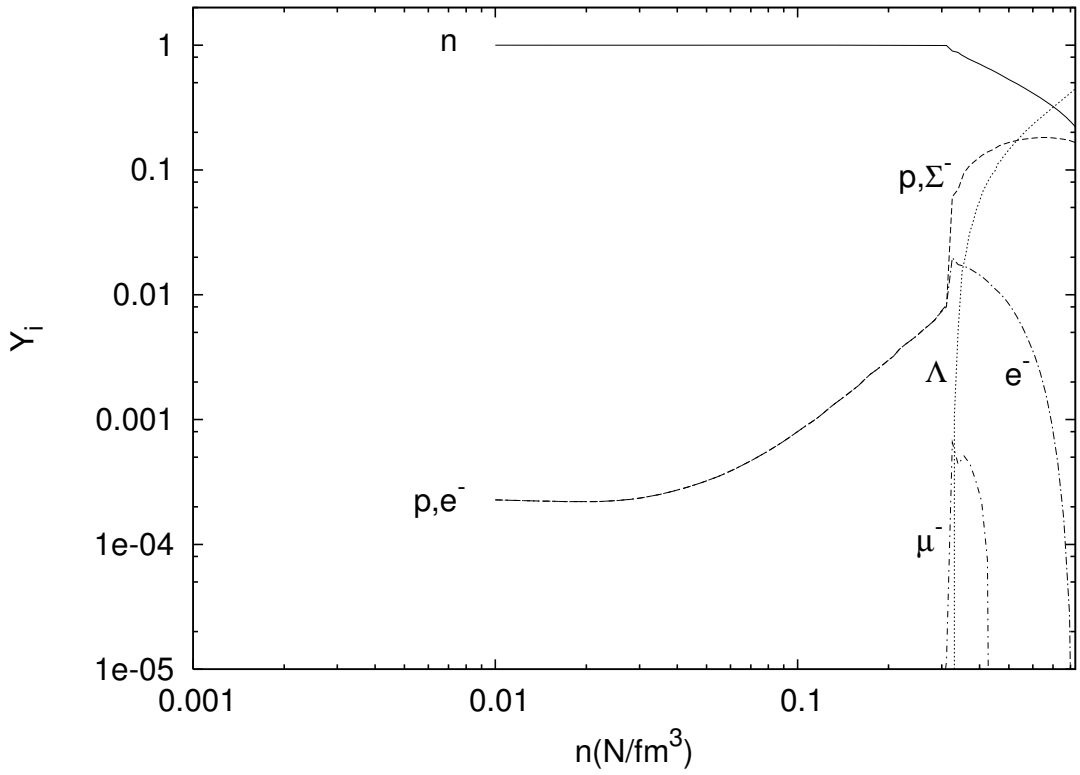

Figure 5.22: Composition of β-stable nuclear matter.

The first hyperon to appear is the Σ^-. It appears together with the μ at $n = 0.32\mathrm{fm}^{-3}$. The Λ follows closely at $n = 0.33\mathrm{fm}^{-3}$. The muon disappears quite quickly. The Σ^-

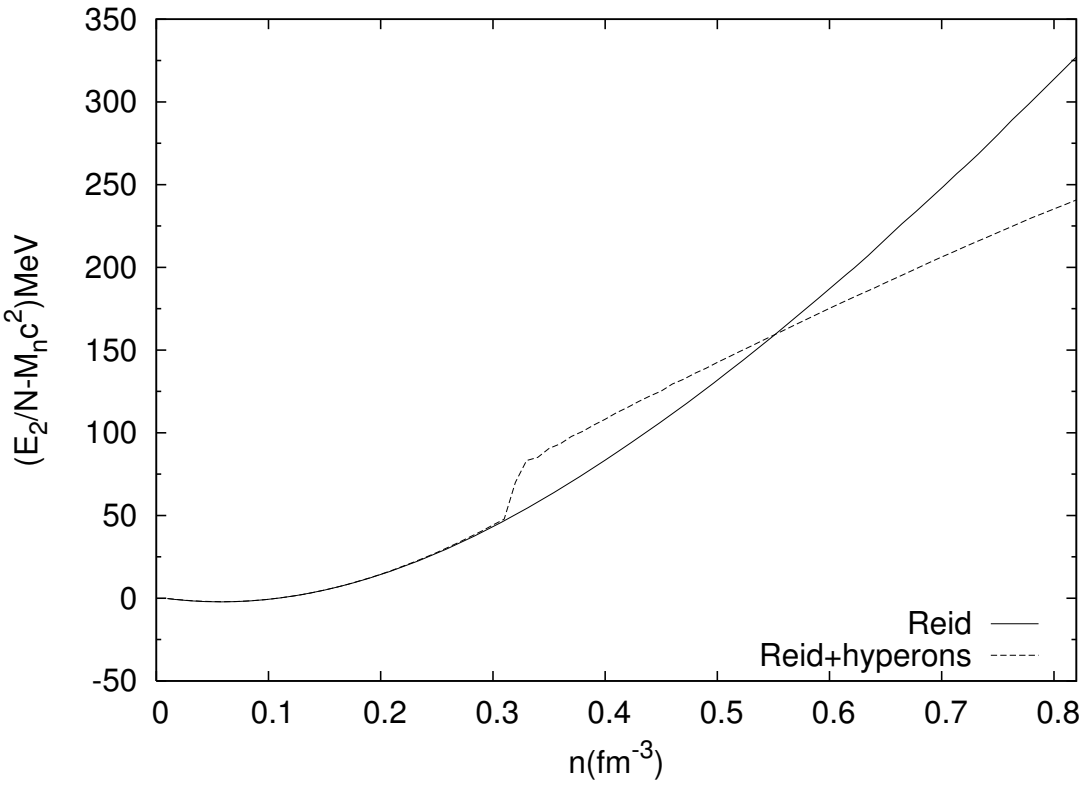

Figure 5.23: Energy as function of number density.

concentration grows fast at the expense of the electron which concentration decreases rapidly. The Σ^- concentrations starts tracing the proton concentration and stabilizes. The Λ concentrations keeps on rising leading to a sharp decrease in the neutron concentration. At a density of $n = 0.82\mathrm{fm}^{-3}$ the electron effectively disappears from the liquid and one is left with neutrons, protons Σ^-'s and Λ's.

The Energy per baryon Fig. 5.23 which has a minimum at low density increases with higher densities. When the hyperons appear in the fermion liquid, the energy per baryon increases sharply. It reaches a higher energy per baryon than the fermion liquid without hyperons. After this short jump the energy starts increasing monotonically with increasing densities and at higher density it has a smaller energy per baryon than the liquid without hyperons.

Finally the equation of state for β-stable hyperon matter is given in Fig. 5.24. As a comparison also are shown the EoS of β-stable matter and the EoS of neutron matter.

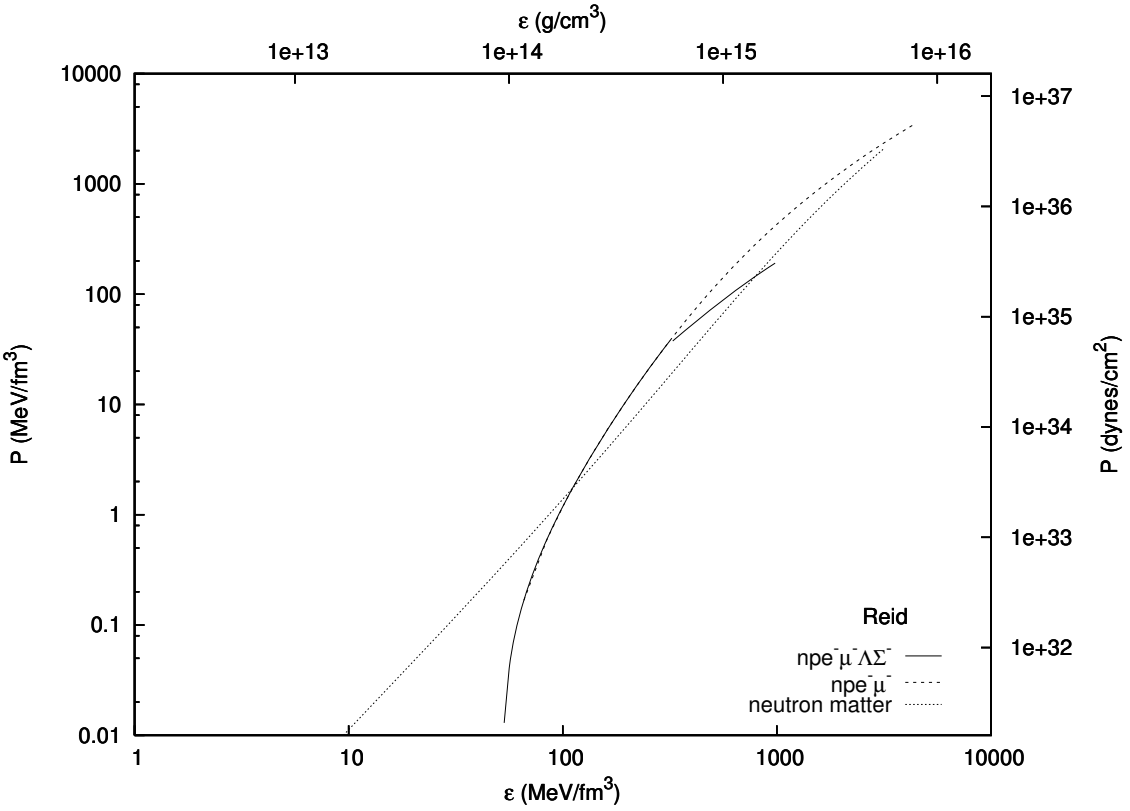

Figure 5.24: Equation of state with Reid potential of β-stable hyperon matter.

At first there is no difference between the EoS of β-stable nuclear and hyperon matter. They are both stiffer then the EoS of neutron matter. When the first hyperons appear the EoS of β-stable hyperon matter softens a bit, compared to the EoS of nuclear matter. The EoS of hyperon matter crosses the EoS of neutron matter just at the point the LOCV calculation fails.

5.7 Neutron star models

The EoS of the previous section can be used in the TOV-equation to create a model for a neutron star. The TOV-equation is solved for different central densities and the resulting mass and radius is plotted in Fig. 5.25. For all three EoS's the mass of a neutron star

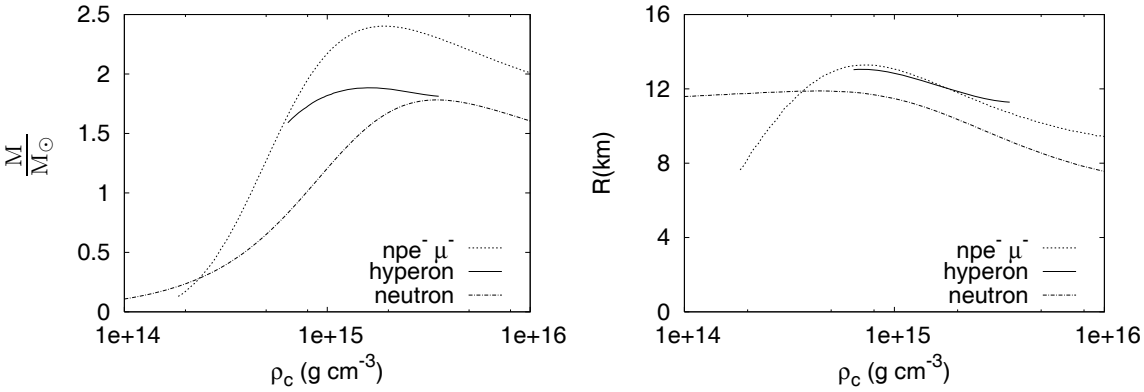

Figure 5.25: Radius and total mass versus central density for β-stable nuclear and hyperon matter and neutron matter.

increases with increasing central density up to a maximum mass and the mass starts to decrease very slowly afterwards. The different maximum masses and the corresponding central densities are tabulated in Table 5.4. Compared to the results of Chapter 2 this

	$npe^-\mu^-$	hyperon	neutron
maximum mass($M_\odot$)	2.40	1.80	1.78
central density(gcm^{-3})	1.9×10^{14}	9.4×10^{14}	3.5×10^{15}

Table 5.4: Maximum mass and corresponding central density for β-stable nuclear and hyperon matter and neutron matter.

are more massive neutron stars. This again is a result from the strong repulsive Reid potential. For central densities up to $6 \times 10^{14}\mathrm{gcm}^{-3}$ there is no difference between β-stable nuclear and hyperon matter. This is not surprising because this is still in the density region where no hyperons appear. Above this density when the hyperons appear the mass of neutron star increases much more slowly with increasing central density compared to nuclear matter. Lastly in Fig. 5.26 the mass versus the radius is plotted for the maximum mass stars for the three EoS's.

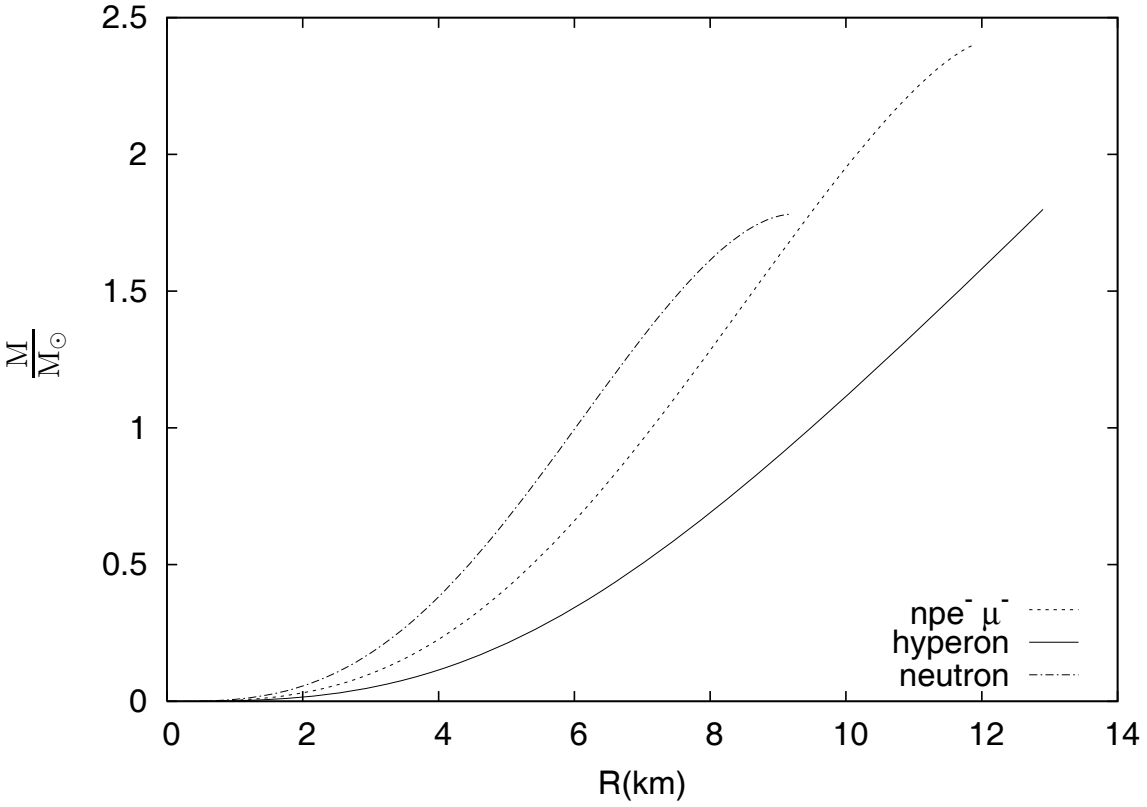

Figure 5.26: Mass versus radius for maximum mass star.